The 8th European Congress on Computational Methods in Applied Sciences and Engineering
ECCOMAS Congress 2022
5-9 June 2022, Oslo, Norway

A LEVEL-SET MODEL FOR TWO-PHASE FLOW WITH VARIABLE SURFACE TENSION: THERMOCAPILLARITY AND SURFACTANTS

N. Balcázar-Arciniega[1,*], J. Rigola[1] and A. Oliva[1]

[1,*] Heat and Mass Transfer Technological Centre (CTTC),
Universitat Politècnica de Catalunya - BarcelonaTech (UPC),
ESEIAAT, Colom 11, 08222 Terrassa (Barcelona), Spain.
{nestor.balcazar, joaquim.rigola, asensio.oliva}@upc.edu

Key words: Unstructured Conservative Level-Set Method, Unstructured Flux-Limiters, Finite-Volume Method, Unstructured Meshes, Variable Surface Tension, Thermocapillarity, Surfactants

Abstract. An unstructured conservative level-set method for two-phase flow with variable surface tension is introduced. Surface tension is a function of temperature or surfactant concentration on the interface. Consequently, the called Marangoni stresses induced by temperature gradients or surfactant concentration gradients on the interface lead to a coupling of momentum transport equation with thermal energy transport equation or interface surfactant transport equation. The finite-volume method discretizes transport equations on 3D collocated unstructured meshes. The unstructured conservative level-set method is employed for interface capturing, whereas the multiple marker approach avoids the numerical coalescence of fluid particles. The fractional-step projection method solves the pressure-velocity coupling. Unstructured flux-limiters are proposed to discretize the convective term of transport equations. A central difference scheme discretizes diffusive terms. Gradients are evaluated by the weighted least-squares method. Verifications and validations are reported.

1 INTRODUCTION

Applications of transport phenomena in two-phase flow are omnipresent in nature and industry. Diverse engineering systems, from nuclear reactors to internal combustion engines, from unit operations and chemical reactors in chemical processing plants to sediment and pollutant transport phenomena in aquatic environments, entail carrier fluids that convey bubbles or droplets of another phase. The design and optimization of these systems and their operation require a deep understanding of the fundamentals of momentum, energy and mass transport processes from individual bubbles and droplets, as well as in swarms of fluid particles.

In this sense, multiple methods have been reported for DNS of two-phase flows, which can be categorized based on the underlying scheme used for the advection of the fluid interface, such as: level-set (LS) [30, 39, 23], Volume of Fluid (VoF) [24, 33, 45, 31], coupled VoF-LS [38, 37, 9], conservative level-set (CLS) [29, 7, 14], and front-tracking (FT) [46, 44]. Although these methods share a similar idea, their numerical implementations on structured or unstructured meshes are quite different [14, 9, 8, 7].

Some of the aforementioned interface capturing/tracking methods have been extended to deal with two-phase flows with variable surface tension. For instance, Balcazar et al.[12] reported thermocapillary

migration of individual and multiple droplets employing a novel multiple marker conservative level-set method. [28, 27] performed direct numerical simulations of the thermocapillary motion of multiple deformable droplets employing the front-tracking method. [25, 34] reported direct simulations of thermal Marangoni effects at deformable interfaces, based on the volume-of-fluid method. [47, 18] reported simulations of the thermocapillary motion of two- and three-dimensional fluid particles using the level-set method. [26] introduced a front-tracking method for insoluble and soluble surfactants. Although previous efforts have reported remarkable numerical and physical findings, many other configurations and flow conditions are not explored yet. This work is a systematic step toward designing numerical methods for complex interfacial physics in the framework of the unstructured multiphase level-set solver proposed by Balcazar et al.[14, 13, 4, 6, 12, 8, 7], for two-phase flow with variable surface tension.

This paper is organized as follows: Section 2 presents the mathematical formulation and the numerical methodology on collocated unstructured meshes. Verifications, validations and numerical experiments are presented in Section 3. Finally, conclusions are remarked in Section 4.

2 MATHEMATICAL FORMULATION AND NUMERICAL METHODS

2.1 Incompressible two-phase flow

The Navier-Stokes equations for the dispersed fluid (Ω_d) and continuous fluid (Ω_c) are presented in the framework of the one-fluid formulation [45, 31],

$$\frac{\partial}{\partial t}(\rho \mathbf{v}) + \nabla \cdot (\rho \mathbf{v}\mathbf{v}) = -\nabla p + \nabla \cdot \mu(\nabla \mathbf{v}) + \nabla \cdot \mu(\nabla \mathbf{v})^T + (\rho - \rho_0)\mathbf{g} + \mathbf{f}_\sigma, \tag{1}$$

$$\nabla \cdot \mathbf{v} = 0. \tag{2}$$

Here, $\mathbf{v}$ is the velocity field, p is the pressure, $\mathbf{g}$ is the gravitational acceleration, μ is the dynamic viscosity, ρ is the fluid density, $\mathbf{f}_\sigma$ is the surface tension force per unit volume acting on the interface Γ, subscripts d and c denote the continuous phase and dispersed phase respectively. Physical properties are constant at each fluid phase, with a jump discontinuity across the interface:

$$\rho = \rho_c H_c + \rho_d H_d, \; \mu = \mu_c H_c + \mu_d H_d. \tag{3}$$

H_c denotes the Heaviside step function, equal to one at the fluid c (Ω_c) and zero elsewhere. $H_d = 1 - H_c$. If periodic boundary conditions are applied in the vertical direction (parallel to $\mathbf{g}$), the force $-\rho_0 \mathbf{g}$ with $\rho_0 = V_\Omega^{-1} \int_\Omega (\rho_d H_d + \rho_c H_c)\, dV$, is included in Eq.(1) [14, 6, 8].

2.2 Multiple marker UCLS method

Interface capturing is performed by the unstructured conservative level-set (UCLS) method, proposed by Balcazar et al.[14, 7]. The multiple marker UCLS approach introduced in Balcazar et al.[14, 4, 6, 12, 8] avoids the numerical coalescence of bubbles. Each marker is represented by a modified level-set function [14, 12, 7], $\phi_i = 0.5\,(\tanh(d_i/(2\varepsilon)) + 1)$, where d_i is a signed distance function [30, 40], ε is a parameter that sets the thickness of the interface profile. The transport equation for the ith level-set marker is written in conservative form:

$$\frac{\partial \phi_i}{\partial t} + \nabla \cdot \phi_i \mathbf{v} = 0, \; i = 1, 2, ..., N_m, \tag{4}$$

where N_m is the number of level-set markers, here equivalent to the number of fluid particles $N_m = n_d$. A re-initialization equation has to be solved to keep a sharp and constant interface profile [7]:

$$\frac{\partial \phi_i}{\partial \tau} + \nabla \cdot \phi_i(1-\phi_i)\mathbf{n}_i^0 = \nabla \cdot \varepsilon \nabla \phi_i,\ i = 1,2,...,N_m. \tag{5}$$

Eq.(5) is advanced in pseudo-time τ up to the steady-state. Here, $\mathbf{n}_i^0$ denotes the interface normal unit vector at $\tau = 0$. At the cell Ω_P, $\varepsilon_P = 0.5(h_P)^\alpha$, $\alpha = 0.9$, $h_P = \max\{||\mathbf{x}_F - \mathbf{x}_P||\}$ is the local grid size [14, 12, 7], subindex P is the local cell, subindex $F = \{1,...,N_f\}$ is the neighbor cell, Normal vectors $\mathbf{n}_i$ and interface curvatures κ_i, are evaluated as: $\mathbf{n}_i = \nabla\phi_i/||\nabla\phi_i||$, $\kappa_i = -\nabla \cdot \mathbf{n}_i$ [14, 8, 7].

2.3 Variable surface tension

Surface tension force ($\mathbf{f}_\sigma$, Eq.(1)) is computed in the framework of the Continuous Surface Force (CSF) model [17], extended to the multiple marker UCLS method in Balcazar et al. [8, 12, 21, 6, 14]:

$$\mathbf{f}_\sigma = \sum_{i=1}^{N_m} (\mathbf{f}_{\sigma,i}^{(n)} + \mathbf{f}_{\sigma,i}^{(t)}), \tag{6}$$

where $\mathbf{f}_{\sigma,i}^{(n)}$ is the normal component of the surface tension force, perpendicular to the interface (Γ_i):

$$\mathbf{f}_{\sigma,i}^{(n)} = \sigma\kappa_i\mathbf{n}_i\delta_{\Gamma,i}^s = \sigma\kappa_i\mathbf{n}_i||\nabla\phi_i|| = \sigma\kappa_i\nabla\phi_i. \tag{7}$$

Here, $\delta_{\Gamma,i}^s = ||\nabla\phi_i||$ is the regularized Dirac delta function concentrated at the interface [14, 7, 6]. Furthermore, $\sigma = \sigma(\varphi)$ is the surface tension coefficient as a function of $\varphi = \{T, C_\Gamma\}$, where T denotes the temperature and C_Γ is the concentration of surfactant on the interface. The second component of Eq.(6), $\mathbf{f}_{\sigma,i}^{(t)}$, is the so-called Marangoni force [20], which is tangential to the interface:

$$\mathbf{f}_{\sigma,i}^{(t)} = \nabla_{\Gamma_i}\sigma(\varphi)\delta_{\Gamma,i}^s = (\nabla\sigma(\varphi) - \mathbf{n}_i(\mathbf{n}_i \cdot \nabla\sigma(\varphi)))\delta_{\Gamma,i}^s = (\nabla\sigma(\varphi) - \mathbf{n}_i(\mathbf{n}_i \cdot \nabla\sigma(\varphi)))||\nabla\phi_i||, \tag{8}$$

where $\nabla_{\Gamma_i} = \nabla - \mathbf{n}_i(\mathbf{n}_i \cdot \nabla)$, is the tangential component of the gradient operator on the interface Γ_i.

2.4 Thermocapillarity

As the critical temperature for a given fluid is approached, the properties of the liquid and vapor phases become identical. Consequently, $\partial\sigma(T)/\partial T = \sigma_T$ and $\sigma_T < 0$. Moreover, the equation of state for surface tension is almost linear for most fluids:

$$\sigma = \sigma(T) = \sigma_0 + \sigma_T(T - T_0), \tag{9}$$

with $\sigma_0 = \sigma(T_0) > 0$. Combination of Eq.(9) and Eq.(8), with $\varphi = T$, leads to the Marangoni force [12]:

$$\mathbf{f}_{\sigma,i}^{(t)} = \mathbf{f}_{\sigma,i}^{(t)}(T) = (\sigma_T\nabla T - \sigma_T\mathbf{n}_i(\mathbf{n}_i \cdot \nabla T))||\nabla\phi_i||, \tag{10}$$

which is valid for thermocapillary migration of fluid particles [12], when $\sigma(T)$ is linear. Finally, temperature field $T(\mathbf{x},t)$ evolves according to the energy transport equation [12]:

$$\rho c_p \left(\frac{\partial T}{\partial t} + \nabla \cdot (\mathbf{v}T)\right) = \nabla \cdot (\lambda \nabla T), \tag{11}$$

where $\lambda = \lambda_d H_d + \lambda_c H_c$ defines the thermal conductivity in the whole domain Ω, and $c_p = c_{p,d} H_d + c_{p,c} H_c$ is the specific heat capacity.

2.5 Insoluble surfactants on the interface

If $\sigma = \sigma(C_\Gamma)$, the Marangoni force is defined by Eq.(8) with $\varphi = C_\Gamma$. Multiple equations of state $\sigma = \sigma(C_\Gamma)$ are proposed in the literature, e.g., [26]. Insoluble surfactant concentration on the interface evolves according to the transport equation [36]:

$$\frac{\partial C_\Gamma}{\partial t} + \nabla_\Gamma \cdot (C_\Gamma \mathbf{v}_\Gamma) + C_\Gamma (\nabla_\Gamma \cdot \mathbf{n})(\mathbf{v} \cdot \mathbf{n}) = \mathcal{D}_\Gamma \nabla_\Gamma^2 C_\Gamma \tag{12}$$

where $\mathcal{D}_\Gamma$ is the surfactant diffusivity. An equivalent transport equation was derived by [42, 43], which is written in the framework of the multiple markers approach:

$$\frac{\partial}{\partial t}(\delta^s_{\Gamma,i} C_\Gamma) + \nabla \cdot (\delta^s_{\Gamma,i} C_\Gamma \mathbf{v}) = \mathcal{D}_\Gamma \nabla \cdot (\delta^s_{\Gamma,i} \nabla C_\Gamma), \tag{13}$$

where $\delta^s_{\Gamma,i} = ||\nabla \phi_i||$ is the regularized Dirac delta function [14, 6].

2.6 Regularization of physical properties

Following [14, 12, 8], fluid properties (Eq.(3)) are regularized with a global level-set function (ϕ). If $H^s_c = \phi$ and $H^s_d = 1 - H^s_c$, then: $\phi = \min\{\phi_1, ..., \phi_{n_d-1}, \phi_{n_d}\}$. Here, $0.5 \leqslant \phi_i \leqslant 1$ in Ω_c, and $0 \leqslant \phi_i < 0.5$ in Ω_d. Alternatively, if $0.5 \leqslant \phi_i \leqslant 1$ in Ω_d, and $0 \leqslant \phi_i < 0.5$ in Ω_c, then $\phi = \max\{\phi_1, ..., \phi_{n_d}\}$, whereas $H^s_d = \phi$ and $H^s_c = 1 - H^s_d$ [14, 8, 6, 12]. Regularization of physical properties for thermocapillary motion of droplets can be found in [12].

2.7 Numerical methods

Transport equations are discretized by the finite-volume method on 3D collocated unstructured meshes [14, 7]. The convective term of momentum equation (Eq.(1)), level-set advection equation (Eq.(4)), interface surfactant concentration equation (Eq.(13)), and thermal equation (Eq.(11)), is explicitly computed, by approximating the fluxes at cell faces with unstructured flux-limiter schemes, proposed by Balcazar et al.[14, 7]. Indeed, a general approximation of the convective term in the cell Ω_P is written as $(\nabla \cdot \beta\psi\mathbf{v})_P = V_P^{-1} \sum_f \beta_f \psi_f (\mathbf{v}_f \cdot \mathbf{A}_f)$, where V_P is the volume of Ω_P, subindex f denotes the cell-faces, $\mathbf{A}_f = ||\mathbf{A}_f|| \mathbf{e}_f$ is the area vector, $\mathbf{e}_f$ is a unit-vector perpendicular to the face f pointing outside the cell Ω_P. Furthermore, $\psi_f = \psi_{C_p} + 0.5 L(\theta_f)(\psi_{D_p} - \psi_{C_p})$, where $L(\theta_f)$ is the flux limiter, $\theta_f = (\psi_{C_p} - \psi_{U_p})/(\psi_{D_p} - \psi_{C_p})$, C_p is the upwind point, U_p is the far-upwind point, and D_p is the downwind point, as proposed in the framework of the UCLS method [14]. Some of the flux limiters implemented on the unstructured multiphase solver [14] have the form [41, 22]:

$$L(\theta_f) \equiv \begin{cases} \max\{0, \min\{2\theta_f, 1\}, \min\{2, \theta_f\}\} & \text{SUPERBEE,} \\ (\theta_f + |\theta_f|)/(1 + |\theta_f|) & \text{VANLEER,} \\ \max\{0, \min\{4\theta_f, 0.75 + 0.25\theta_f, 2\}\} & \text{SMART,} \\ 1 & \text{CD,} \\ 0 & \text{UPWIND.} \end{cases} \tag{14}$$

Compressive term of the re-initialization equation (Eq. (5)), is discretized at the cell Ω_P as follows [14]: $(\nabla \cdot \phi_i(1-\phi_i)\mathbf{n}_i^0)_P = \frac{1}{V_P}\sum_f (\phi_i(1-\phi_i))_f \mathbf{n}_{i,f}^0 \cdot \mathbf{A}_f$, where $\mathbf{n}_{i,f}^0$ and $(\phi_i(1-\phi_i))_f$ are linearly interpolated. The diffusive term of transport equations are centrally differenced [14]. Gradients are computed at cell centroids through the weighted least-squares method [14, 16, 13, 7]. The fractional-step projection method [19, 31, 45] solves the pressure-velocity coupling. First, a predictor velocity ($\mathbf{v}_P^*$) is calculated:

$$\frac{\rho_P \mathbf{v}_P^* - \rho_P^0 \mathbf{v}_P^0}{\Delta t} = \mathbf{C}_{\mathbf{v},P}^0 + \mathbf{D}_{\mathbf{v},P}^0 + (\rho_P - \rho_0)\mathbf{g} + \mathbf{f}_{\sigma,P}, \tag{15}$$

where the super-index 0 denotes the previous time-step, subindex P denotes the control volume Ω_P, $\mathbf{D}_\mathbf{v} = \nabla \cdot \mu \nabla \mathbf{v} + \nabla \cdot \mu (\nabla \mathbf{v})^T$, and $\mathbf{C}_\mathbf{v} = -\nabla \cdot (\rho \mathbf{v}\mathbf{v})$. Imposing $(\nabla \cdot \mathbf{v})_P = 0$ to the corrector step, Eq. (17), leads to a Poisson equation for the pressure at cell-centroids:

$$\left(\nabla \cdot \left(\frac{\Delta t}{\rho}\nabla p\right)\right)_P = (\nabla \cdot \mathbf{v}^*)_P, \ \mathbf{e}_{\partial\Omega} \cdot \nabla p|_{\partial\Omega} = 0. \tag{16}$$

which is solved by means of a preconditioned conjugate gradient method. A Jacobi pre-conditioner is used in this research. Here $\partial\Omega$ denotes the boundary of Ω, excluding regions with periodic boundary condition, where information of the corresponding periodic nodes is used [14, 8]. In a further step the updated velocity ($\mathbf{v}_P$) is computed at cell-centroids:

$$\frac{\rho_P \mathbf{v}_P - \rho_P \mathbf{v}_P^*}{\Delta t} = -(\nabla p)_P. \tag{17}$$

Furthermore, face-cell velocity $\mathbf{v}_f$ is interpolated [12, 14] to fulfill the incompressibility constraint and to avoid pressure-velocity decoupling on collocated meshes [32]. Then, the volume flux ($\mathbf{v}_f \cdot \mathbf{A}_f$), normal velocity ($\mathbf{v}_f \cdot \mathbf{e}_f$) or some equivalent variable is employed to solve the convective term of transport equations [12]. An example of global algorithm for complex interfacial physics and further details on the discretization can be found in our recent works [14, 13, 16].

3 NUMERICAL EXPERIMENTS

3.1 Validations and verifications

Multiple validations, verifications and extensions of the unstructured multiphase flow solver [7, 10, 6, 14, 13] have been reported, for instance: buoyancy-driven rising bubbles [7, 8, 6, 2, 1], thermocapillary-driven motion of droplets on fixed unstructured meshes [12], bubbly flows [11, 6, 14, 15, 16], falling droplets [5], binary droplet collision with bouncing outcome [11], bouncing collision of a droplet against a fluid-fluid interface [11], liquid atomization [35], deformation of droplets under shear stresses [9], interfacial mass transfer in bubbly flows [16, 4, 14, 15], and liquid-vapor phase change [13]. Furthermore, a comparison of the UCLS method [7, 8, 12] and unstructured coupled VoF-LS method [9] is reported in [5].

3.2 Convection of insoluble surfactants on a droplet interface

A similar case was proposed by [26]. The unstructured flux-limiters convective schemes proposed by Balcazar et a.[16, 7] are used on the discretization of the interface surfactant transport equation (Eq.(13)).

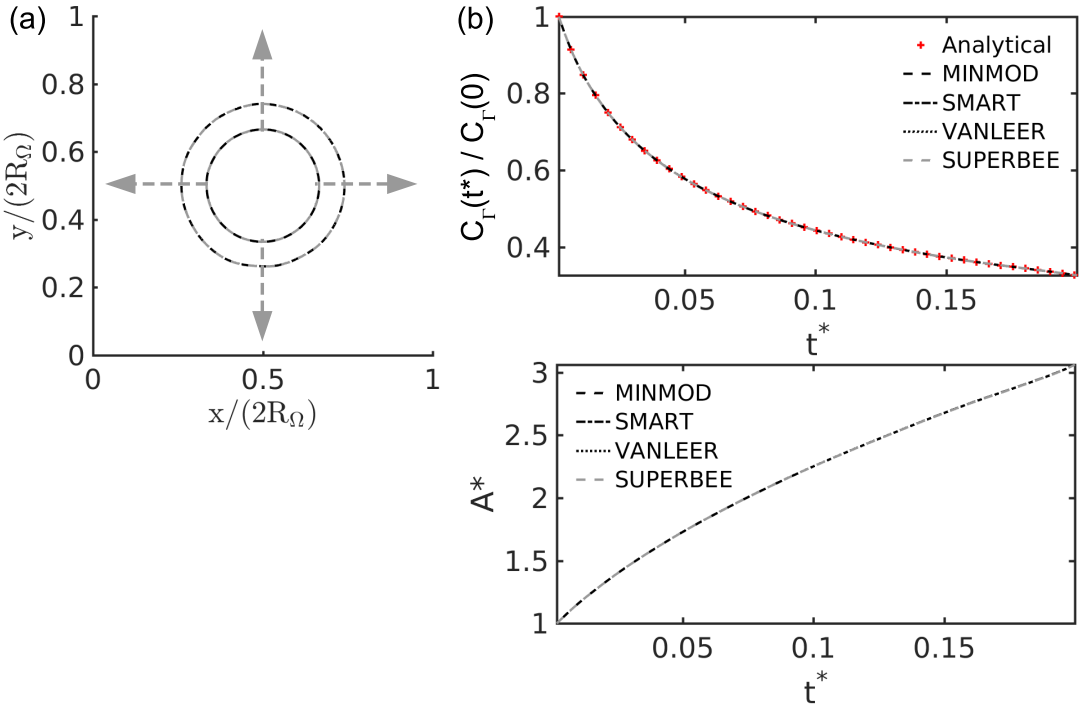

Figure 1: Convection of insoluble surfactants on a droplet interface. (a) Radially expanding interface at $t^* = \{0.01, 0.07\}$. (b) Surfactant concentration of the droplet interface. Analytical solution and numerical results using unstructured flux-limiters convective schemes proposed by Balcazar et al.[14, 13, 16, 7] for MINMOD, SMART, VANLEER and SUPERBEE limiters. Flux-limiters are applied to Eq.(4) and Eq.(13).

Ω is a cylinder of radius $R_\Omega = 3.33(d/2)$ on the plane $x-y$ and thickness $L_z = h$ along the z axis. Here d is the initial droplet diameter. The mesh consists of 18464 triangles on the plane $x-y$ extruded along the z-axis a distance h, which leads to triangular prisms control volumes with an average grid size $h = 2R_\Omega/100$. Only UCLS equations and surfactant transport equations are solved (Eq.(13)).

As the initial condition, a cylindrical droplet of diameter d is located on the symmetry axis of Ω, $\mathbf{x}_0 = (x_0, y_0)$. Furthermore, the surfactant concentration $C_\Gamma(0) = C_\Gamma^0$ is uniformly distributed on the droplet interface. Then, the cylindrical droplet is expanding with a solenoidal and radial velocity $\mathbf{v} = (C/r)\mathbf{e}_r$, with $r = \sqrt{(x-x_0)^2 + (y-y_0)^2}$. The reference length is $L_r = 2R_\Omega$, reference velocity $U_r = C/(0.5d)$, and reference time $t_r = L_r/U_r$, which will be used for the numerical results. The surfactant concentration evolves according to the analytical solution: $C_\Gamma = C_\Gamma^0 A_i(0)/A_i(t)$, where $A_i(t)$ is the interface surface. The numerical results for MINMOD, SMART, VANLEER and SUPERBEE flux limiters are in close agreement with the analytical result, as shown in Figure 1.

3.3 Thermocapillary migration of a droplet

Thermocapillary migration of droplets is characterized by the following dimensionless numbers:

$$Ma = \frac{|\sigma_T|||\nabla T_\infty||d^2\rho_c c_{p,c}}{4\mu_c\lambda_c}, \; Re = \frac{|\sigma_T|||\nabla T_\infty||d^2\rho_c}{4\mu_c^2}, \; Ca = \frac{|\sigma_T|||\nabla T_\infty||d}{2\sigma_0}, \; \eta_\beta = \frac{\beta_c}{\beta_d}. \tag{18}$$

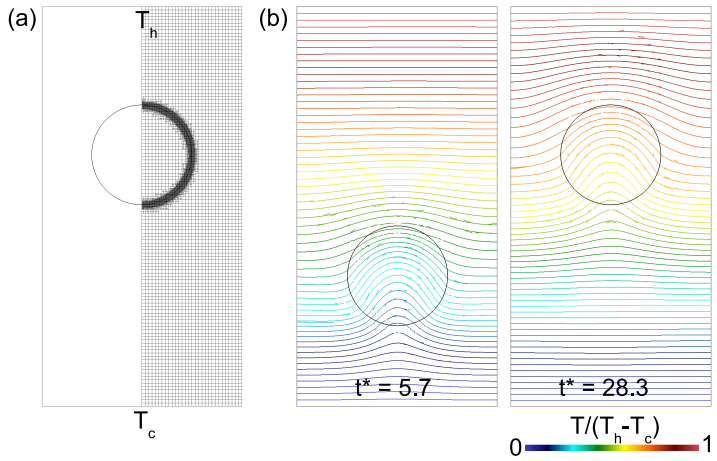

Figure 2: Thermocapillary migration of a droplet: $\mathbf{g} = \mathbf{0}$. $Re = 5.0$, $Ma = 20.0$, $Ca = 0.01666$, $\eta_\rho = \rho_c/\rho_d = 2.0$, $\eta_\mu = \mu_c/\mu_d = 2.0$, $\eta_\lambda = \lambda_c/\lambda_d = 2.0$, $\eta_{c_p} = c_{p,c}/c_{p,d} = 2.0$. (a) Adaptive mesh refinement around the droplet interface, with grid size $h_{max} = L_x/60$ and $h_{min} = h_{max}/2^4$. (b) Temperature contours.

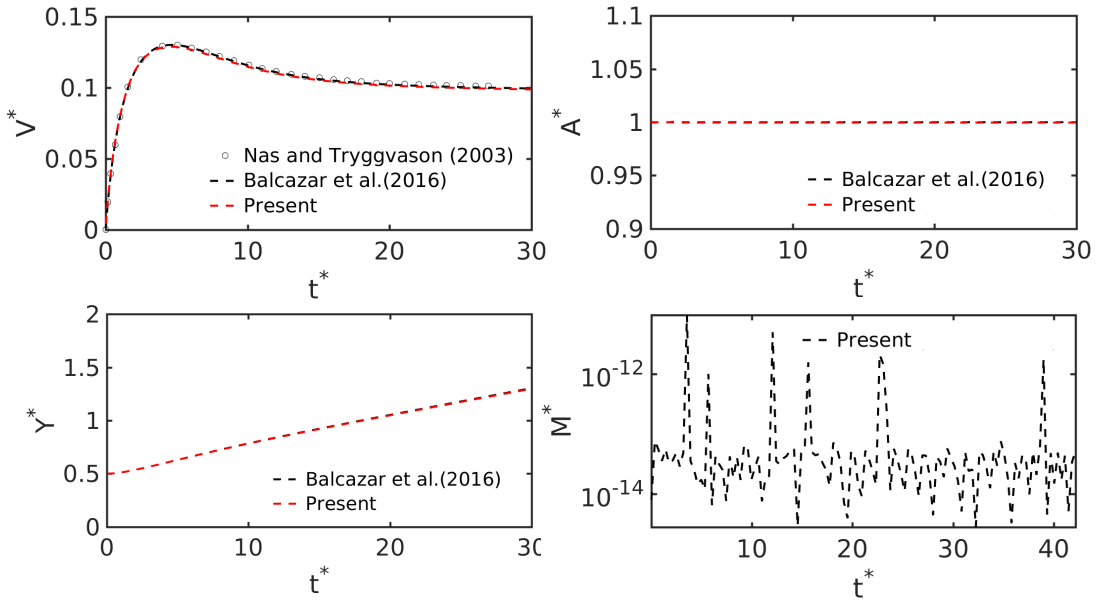

Figure 3: Thermocapillary migration of a droplet: $\mathbf{g} = \mathbf{0}$. $Re = 5.0$, $Ma = 20.0$, $Ca = 0.01666$, $\eta_\rho = \rho_c/\rho_d = 2.0$, $\eta_\mu = \mu_c/\mu_d = 2.0$, $\eta_\lambda = \lambda_c/\lambda_d = 2.0$, $\eta_{c_p} = c_{p,c}/c_{p,d} = 2.0$. Dimensionless migration velocity $V^* = \mathbf{e}_y \cdot \mathbf{v}_{c,i}/U_r$, $\mathbf{v}_{c,i}$ is the droplet velocity. Dimensionless time $t^* = t/t_r$. Normalized droplet surface, $A^* = A_i(t)/A_i(0)$, $A_i(t) = \int_{V_\Omega} \delta^s_{\Gamma,i} dV$, $\delta^s_{\Gamma,i} = ||\nabla \phi_i||$ [7, 11, 12, 9, 6, 14, 13, 16]. Dimensionless vertical position, $Y^* = \mathbf{e}_y \cdot \mathbf{x}_{c,i}/L_x$, $\mathbf{x}_{c,i}$ is the droplet centroid. Mass conservation error $M^* = (M_d(t) - M_d(0))/M_d(0)$, with $M_d(t) = \int_\Omega H^s_d(t) dV$.

where $\beta = \{\rho, \mu, \lambda, c_p\}$, Ma is the Marangoni number, Re is the Reynolds number, Ca is the capillary number, η_β denotes the physical property ratio, $\nabla T_\infty = ((T_h - T_c)/L_y)\mathbf{e}_y$, T_h is the temperature at the top boundary (hot), and T_c is the temperature at the bottom boundary (cold) as shown in Figure 2a. Further-

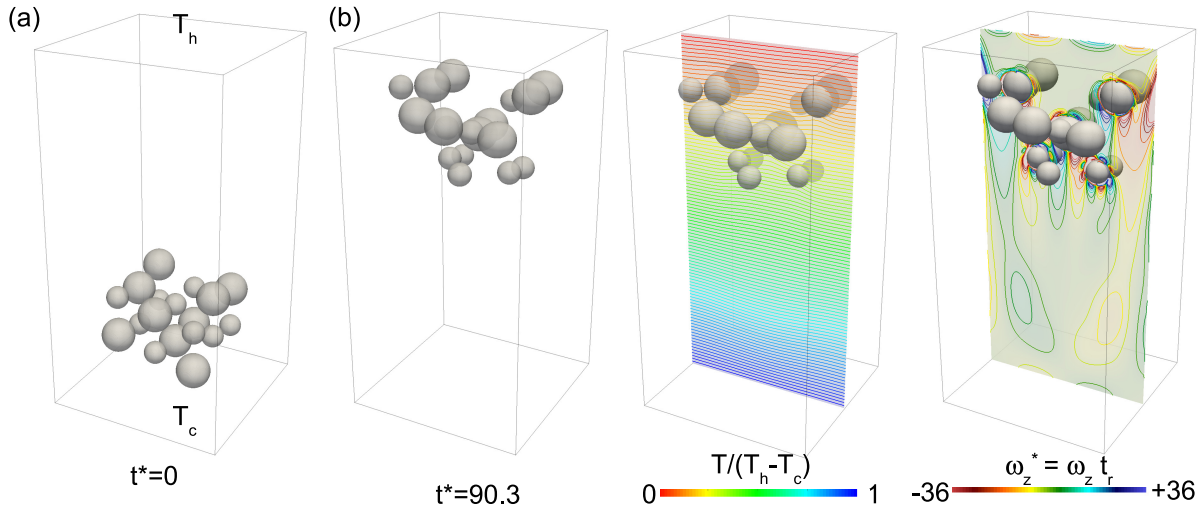

Figure 4: Thermocapillary migration of 18 droplets. $\mathbf{g} = \mathbf{0}$. Dimensionless numbers: $Re = 80$, $Ma = 10$, $Ca = 0.0416$, $\eta_\rho = \rho_c/\rho_d = 2.0$,$\eta_\mu = \mu_c/\mu_d = 2.0$,$\eta_\lambda = \lambda_c/\lambda_d = 2.0$,$\eta_{c_p} = c_{p,c}/c_{p,d} = 2.0$. $\eta_d = d^*/d = 2/3$. Here $\omega_z = \mathbf{e}_z \cdot (\nabla \times \mathbf{v})$.

more, the reference velocity is $U_r = |\sigma_T|||\nabla T_\infty||(0.5d)/\mu_c$, reference temperature $T_r = ||\nabla T_\infty||(0.5d)$, and reference time $t_r = 0.5d/U_r$, which will be employed to present the numerical results.

This case was reported in [28] and successfully solved in Balcazar et al.[12] through the UCLS method on fixed unstructured meshes. Here, the UCLS method [14, 12, 7] for two-phase flow with variable surface tension is proved on the hexahedral Adaptive Mesh Refinement (AMR) strategy of [2]. The hexahedral AMR technique [3] was further optimized for wobbling-regime rising bubbles by [2] in the framework of the UCLS two-phase solver of Balcazar et al.[14, 5, 7].

The dimensionless parameters are $Re = 5$, $Ma = 20$, $Ca = 0.016\bar{6}$ and $\eta_\rho = \eta_\mu = \eta_{c_p} = \eta_\lambda = 2$. Ω a rectangle extending $L_x = 4d$ in the x direction and $L_y = 8d$ in the y direction, where d is the drop diameter. The droplet is initially located to the distance d above the bottom wall, on the vertical symmetry axis of Ω. The top and bottom walls are no-slip boundaries with temperature T_h and $T_c < T_h$, respectively. The lateral boundaries are periodic. Figures 2 and 3 show a close agreement of the present numerical results against those reported by [28] and [12] on fixed meshes, proving that the UCLS solver is able to deal with two-phase flows with variable surface tension on adaptive unstructured meshes.

3.4 Thermocapillary migration of a bi-dispersed droplet swarm

DNS of thermocapillary migration of a bi-dispersed droplet swarm is performed. Ω a rectangular channel with $L_x = 6d$, $L_z = 6d$ on the plane $x-z$, and $L_y = 12d$ in the y axis. A uniform cartesian mesh of $240 \times 240 \times 480$ grid points, equivalent to the grid size $h = d/40$, is employed. 18 droplets are randomly distributed (Fig. 4a). The swarm consists of 9 droplets of diameter d and 9 droplets of diameter d^*. The diameter ratio is $\eta_d = d^*/d = 2/3$. Dimensionless numbers are defined in terms of the droplet diameter d. The fluids are initially quiescent, and the temperature increases linearly from the bottom wall to the top wall. No-slip boundary condition is applied to all the boundaries. Lateral walls are adiabatic, whereas

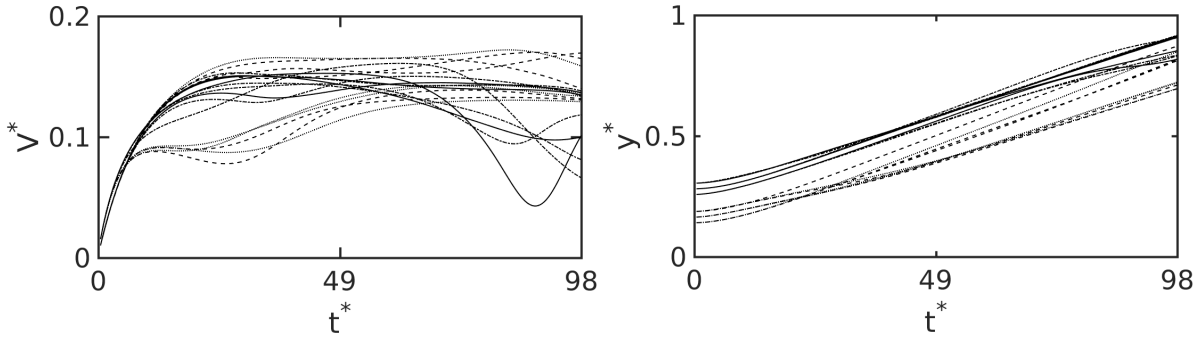

Figure 5: Thermocapillary migration of 18 droplets. Dimensionless migration velocity $V_i^* = \mathbf{e}_y \cdot \mathbf{v}_i / U_r$, $\mathbf{v}_i$ is the velocity of the ith droplet, Dimensionless vertical position, $y_i^* = \mathbf{e}_y \cdot \mathbf{x}_i / L_{y,\Omega}$, $\mathbf{x}_i$ is the centroid of the ith droplet. Dimensionless time $t^* = t/t_r$. $\mathbf{g} = \mathbf{0}$. Dimensionless numbers: $Re = 80$, $Ma = 10$, $Ca = 0.0416$, $\eta_\rho = \rho_c/\rho_d = 2.0$,$\eta_\mu = \mu_c/\mu_d = 2.0$,$\eta_\lambda = \lambda_c/\lambda_d = 2.0$,$\eta_{c_p} = c_{p,c}/c_{p,d} = 2.0$, $\eta_d = d^*/d = 2/3$.

the top and bottom boundaries are at the temperature T_h and $T_c < Th$, respectively. Figures 4-5 show the physical parameters as well as the numerical results, proving the robustness of the UCLS method to perform complex simulations of thermocapillary-driven motion of droplets.

4 CONCLUSIONS

The UCLS method for two-phase flow with variable surface tension on collocated unstructured meshes has been introduced. Validations and verifications include the Marangoni stresses in thermocapillary migration and the convection of surfactants on the interface. Unstructured flux-limiters schemes proposed by Balcazar et al.[14, 7], to discretize the convective term of transport equations, in the framework of the UCLS method, avoids numerical oscillations around the interface and minimize the numerical diffusion. Altogether, numerical schemes have lead to a robust and accurate numerical method for two-phase flows with variable surface tension on collocated unstructured meshes.

ACKNOWLEDGMENTS

The main author, N. Balcázar-Arciniega, as a Serra-Húnter Fellow (UPC-LE8027), acknowledges the Catalan Government for the financial support through this programme. Simulations were executed using computing time granted by the RES (IM-2021-1-0013, IM-2020-2-0002) and PRACE 14th Call (2016153612) on the supercomputer MareNostrum IV based in Barcelona, Spain. The authors acknowledge the financial support of the MINECO, Spain (PID2020-115837RB-100).

REFERENCES

[1] ANTEPARA, O., BALCZAR, N., AND OLIVA, A. Tetrahedral adaptive mesh refinement for twophase flows using conservative levelset method. *International Journal for Numerical Methods in Fluids 93* (2021), 481–503.

[2] ANTEPARA, O., BALCZAR, N., RIGOLA, J., AND OLIVA, A. Numerical study of rising bubbles

with path instability using conservative level-set and adaptive mesh refinement. *Computers and Fluids 187* (2019), 83–97.

[3] ANTEPARA, O., LEHMKUHL, O., BORRELL, R., CHIVA, J., AND OLIVA, A. Parallel adaptive mesh refinement for large-eddy simulations of turbulent flows. *Computers and Fluids 110* (3 2015), 48–61.

[4] BALCÁZAR, N., ANTEPARA, O., RIGOLA, J., AND OLIVA, A. Dns of drag-force and reactive mass transfer in gravity-driven bubbly flows. *In: Garca-Villalba, M., Kuerten, H., Salvetti, M. (eds) Direct and Large Eddy Simulation XII. DLES 2019. ERCOFTAC Series, vol 27. Springer, Cham* (2020), 119–125.

[5] BALCÁZAR, N., CASTRO, J., CHIVA, J., AND OLIVA, A. Dns of falling droplets in a vertical channel. *International Journal of Computational Methods and Experimental Measurements 6* (11 2017), 398–410.

[6] BALCÁZAR, N., CASTRO, J., RIGOLA, J., AND OLIVA, A. Dns of the wall effect on the motion of bubble swarms. *Procedia Computer Science 108* (2017), 2008–2017.

[7] BALCÁZAR, N., JOFRE, L., LEHMKUHL, O., CASTRO, J., AND RIGOLA, J. A finite-volume/level-set method for simulating two-phase flows on unstructured grids. *International Journal of Multiphase Flow 64* (2014), 55–72.

[8] BALCÁZAR, N., LEHMKUHL, O., JOFRE, L., AND OLIVA, A. Level-set simulations of buoyancy-driven motion of single and multiple bubbles. *International Journal of Heat and Fluid Flow 56* (2015).

[9] BALCÁZAR, N., LEHMKUHL, O., JOFRE, L., RIGOLA, J., AND OLIVA, A. A coupled volume-of-fluid/level-set method for simulation of two-phase flows on unstructured meshes. *Computers and Fluids 124* (2016), 12–29.

[10] BALCÁZAR, N., LEHMKUHL, O., JOFRE, L., RIGOLA, J., AND OLIVA, A. A coupled volume-of-fluid/level-set method for simulation of two-phase flows on unstructured meshes. *Computers & Fluids 124* (2016), 12–29.

[11] BALCÁZAR, N., LEHMKUHL, O., RIGOLA, J., AND OLIVA, A. A multiple marker level-set method for simulation of deformable fluid particles. *International Journal of Multiphase Flow 74* (2015), 125–142.

[12] BALCÁZAR, N., RIGOLA, J., CASTRO, J., AND OLIVA, A. A level-set model for thermocapillary motion of deformable fluid particles. *International Journal of Heat and Fluid Flow 62* (12 2016), 324–343.

[13] BALCAZAR, N., RIGOLA, J., AND OLIVA, A. Unstructured level-set method for saturated liquid-vapor phase change. *In: WCCM-ECCOMAS 2020. Volume 600 - Fluid Dynamics and Transport Phenomena.* (2021), 1–12.

[14] BALCÁZAR-ARCINIEGA, N., ANTEPARA, O., RIGOLA, J., AND OLIVA, A. A level-set model for mass transfer in bubbly flows. *International Journal of Heat and Mass Transfer 138* (2019), 335–356.

[15] BALCÁZAR-ARCINIEGA, N., RIGOLA, J., AND OLIVA, A. Dns of mass transfer from bubbles

rising in a vertical channel. *Lecture Notes in Computer Science (including subseries Lecture Notes in Artificial Intelligence and Lecture Notes in Bioinformatics) 11539 LNCS* (2019), 596–610.

[16] BALCÁZAR-ARCINIEGA, N., RIGOLA, J., AND OLIVA, A. Dns ofmass transfer in bi-dispersed bubble swarms. *In: Computational Science ICCS 2022. ICCS 2022. Lecture Notes in Computer Science, vol 13353. Springer, Cham 13353* (2022), 284–296.

[17] BRACKBILL, J. U., KOTHE, D. B., AND ZEMACH, C. A continuum method for modeling surface tension. *Journal of Computational Physics 100* (1992), 335–354.

[18] BRADY, P. T., HERRMANN, M., AND LOPEZ, J. M. Confined thermocapillary motion of a three-dimensional deformable drop. *Physics of Fluids 23* (2 2011), 022101.

[19] CHORIN, A. J. Numerical solution of the navier-stokes equations. *Mathematics of Computation 22* (1968), 745.

[20] DEEN, W. *Analysis of Transport Phenomena*. OXFORD UNIV PR, 2011.

[21] FRDE, F., GRENGA, T., CHENADEC, V. L., BODE, M., AND PITSCH, H. A three-dimensional cell-based volume-of-fluid method for conservative simulations of primary atomization. *Journal of Computational Physics 465* (9 2022), 111374.

[22] GASKELL, P. H., AND LAU, A. K. C. Curvature-compensated convective transport: Smart, a new boundedness- preserving transport algorithm. *International Journal for Numerical Methods in Fluids 8* (1988), 617–641.

[23] GIBOU, F., FEDKIW, R., AND OSHER, S. A review of level-set methods and some recent applications. *Journal of Computational Physics 353* (1 2018), 82–109.

[24] HIRT, C., AND NICHOLS, B. Volume of fluid (vof) method for the dynamics of free boundaries. *Journal of Computational Physics 39* (1 1981), 201–225.

[25] MA, C., AND BOTHE, D. Direct numerical simulation of thermocapillary flow based on the volume of fluid method. *International Journal of Multiphase Flow 37* (11 2011), 1045–1058.

[26] MURADOGLU, M., AND TRYGGVASON, G. A front-tracking method for computation of interfacial flows with soluble surfactants. *Journal of Computational Physics 227* (2 2008), 2238–2262.

[27] NAS, S., MURADOGLU, M., AND TRYGGVASON, G. Pattern formation of drops in thermocapillary migration. *International Journal of Heat and Mass Transfer 49* (7 2006), 2265–2276.

[28] NAS, S., AND TRYGGVASON, G. Thermocapillary interaction of two bubbles or drops. *International Journal of Multiphase Flow 29* (7 2003), 1117–1135.

[29] OLSSON, E., AND KREISS, G. A conservative level set method for two phase flow. *Journal of Computational Physics 210* (11 2005), 225–246.

[30] OSHER, S., AND SETHIAN, J. A. Fronts propagating with curvature-dependent speed: Algorithms based on hamilton-jacobi formulations. *Journal of Computational Physics 79* (11 1988), 12–49.

[31] PROSPERETTI, A., AND TRYGGVASON, G. *Computational Methods for Multiphase Flow*. Cambridge University Press, 2007.

[32] RHIE, C. M., AND CHOW, W. L. Numerical study of the turbulent flow past an airfoil with trailing

edge separation. *AIAA Journal 21* (1983), 1525–1532.

[33] RIDER, W. J., AND KOTHE, D. B. Reconstructing volume tracking. *Journal of Computational Physics 141* (4 1998), 112–152.

[34] SAMAREH, B., MOSTAGHIMI, J., AND MOREAU, C. Thermocapillary migration of a deformable droplet. *International Journal of Heat and Mass Transfer 73* (6 2014), 616–626.

[35] SCHILLACI, E., ANTEPARA, O., BALCZAR, N., SERRANO, J. R., AND OLIVA, A. A numerical study of liquid atomization regimes by means of conservative level-set simulations. *Computers and Fluids 179* (2019), 137–149.

[36] STONE, H. A. A simple derivation of the timedependent convectivediffusion equation for surfactant transport along a deforming interface. *Physics of Fluids A: Fluid Dynamics 2* (1 1990), 111–112.

[37] SUN, D., AND TAO, W. A coupled volume-of-fluid and level set (voset) method for computing incompressible two-phase flows. *International Journal of Heat and Mass Transfer 53* (1 2010), 645–655.

[38] SUSSMAN, M., AND PUCKETT, E. G. A coupled level set and volume-of-fluid method for computing 3d and axisymmetric incompressible two-phase flows. *Journal of Computational Physics 162* (8 2000), 301–337.

[39] SUSSMAN, M., SMEREKA, P., AND OSHER, S. A level set approach for computing solutions to incompressible two-phase flow. *Journal of Computational Physics 114* (9 1994), 146–159.

[40] SUSSMAN, M., SMEREKA, P., AND OSHER, S. A level set approach for computing solutions to incompressible two-phase flow. *Journal of Computational Physics 114* (9 1994), 146–159.

[41] SWEBY, P. K. High resolution schemes using flux limiters for hyperbolic conservation laws. *SIAM Journal on Numerical Analysis 21* (10 1984), 995–1011.

[42] TEIGEN, K. E., LI, X., LOWENGRUB, J., WANG, F., AND VOIGT, A. A diffuse-interface approach for modelling transport, diffusion and adsorption/desorption of material quantities on a deformable interface. *Communications in Mathematical Sciences 7* (2009), 1009–1037.

[43] TEIGEN, K. E., SONG, P., LOWENGRUB, J., AND VOIGT, A. A diffuse-interface method for two-phase flows with soluble surfactants. *Journal of Computational Physics 230* (2011), 375–393.

[44] TRYGGVASON, G., BUNNER, B., ESMAEELI, A., JURIC, D., AL-RAWAHI, N., TAUBER, W., HAN, J., NAS, S., AND JAN, Y.-J. A front-tracking method for the computations of multiphase flow. *Journal of Computational Physics 169* (5 2001), 708–759.

[45] TRYGGVASON, G., SCARDOVELLI, R., AND ZALESKI, S. *Direct numerical simulations of Gas-Liquid multiphase flows*. 2011.

[46] UNVERDI, S. O., AND TRYGGVASON, G. A front-tracking method for viscous, incompressible, multi-fluid flows. *Journal of Computational Physics 100* (5 1992), 25–37.

[47] ZHAO, J.-F., LI, Z.-D., LI, H.-X., AND LI, J. Thermocapillary migration of deformable bubbles at moderate to large marangoni number in microgravity. *Microgravity Science and Technology 22* (9 2010), 295–303.